NASA TECHNICAL NOTE

NASA TN D-5464

NASA TN D-5464

SIMULATION OF PYROLYSIS-GAS FLOW THROUGH A CHAR LAYER DURING ABLATION

by Ronald K. Clark

Langley Research Center
Langley Station, Hampton, Va.

NATIONAL AERONAUTICS AND SPACE ADMINISTRATION • WASHINGTON, D. C. • OCTOBER 1969

1. Report No. NASA TN D-5464	2. Government Accession No.	3. Recipient's Catalog No.
4. Title and Subtitle SIMULATION OF PYROLYSIS-GAS FLOW THROUGH A CHAR LAYER DURING ABLATION		5. Report Date October 1969
		6. Performing Organization Code
7. Author(s) Ronald K. Clark		8. Performing Organization Report No. L-5401
		10. Work Unit No. 124-07-13-01-23
9. Performing Organization Name and Address NASA Langley Research Center Hampton, Va. 23365		11. Contract or Grant No.
		13. Type of Report and Period Covered Technical Note
12. Sponsoring Agency Name and Address National Aeronautics and Space Administration Washington, D.C. 20546		14. Sponsoring Agency Code

15. Supplementary Notes

16. Abstract

An experimental study was made to provide some insight into the complex thermochemical phenomena occurring during the flow of pyrolysis gases through an ablator char layer. Resistance-heated porous carbon slabs were used to simulate ablator char layers, and mixtures of methane and helium, simulating pyrolysis gases, were passed through the heated carbon. Tests were made with carbon temperatures up to approximately 3800^{0} R (2100 K) with various mass flow rates, methane concentrations, and carbon thicknesses for two different porosities. Temperatures of the entrance and exit surfaces of the carbon were measured, and gas temperatures and temperature profiles through the carbon were calculated by a simplified analysis. Gas samples were taken at the exit surface of the carbon and analyzed to determine the hydrogen mole fraction which was used as an index to the extent of gas-phase reactions. Postexposure metallographic analyses of the carbon specimens were made to investigate the deposition of carbon in the specimen voids. Principal conclusions from this study are (1) the methane reacts to form hydrogen, solid carbon, and traces of ethylene and acetylene; (2) a transition region of small temperature range exists below which the gas composition is frozen and above which the composition is in chemical equilibrium; (3) the transition region occurs at lower temperatures with greater carbon internal areas; (4) significant amounts of laminar-type carbon, not resulting from gas-phase reactions, were deposited in the specimen voids; and (5) the gas and solid temperatures apparently did not equilibrate until the gases approached the exit surface of the carbon.

17. Key Words Suggested by Author(s) Pyrolysis Ablation chars Methane decomposition Flow through porous media	18. Distribution Statement Unclassified – Unlimited

19. Security Classif. (of this report)	20. Security Classif. (of this page)	21. No. of Pages	22. Price*
Unclassified	Unclassified	37	$3.00

*For sale by the Clearinghouse for Federal Scientific and Technical Information Springfield, Virginia 22151

SIMULATION OF PYROLYSIS-GAS FLOW THROUGH A CHAR LAYER DURING ABLATION

By Ronald K. Clark
Langley Research Center

SUMMARY

An experimental study was made to provide some insight into the complex thermochemical phenomena occurring during the flow of pyrolysis gases through an ablator char layer. Resistance-heated porous carbon slabs were used to simulate ablator char layers, and mixtures of methane and helium, simulating pyrolysis gases, were passed through the heated carbon. Tests were made with carbon temperatures up to approximately 3800° R (2100 K) with various mass flow rates, methane concentrations, and carbon thicknesses for two different porosities.

Temperatures of the entrance and exit surfaces of the carbon were measured, and gas temperatures and temperature profiles through the carbon were calculated by a simplified analysis. Gas samples were taken at the exit surface of the carbon and analyzed to determine the hydrogen mole fraction, which was used as an index to the extent of gas-phase reactions. Postexposure metallographic analyses of the carbon specimens were made to investigate the deposition of carbon in the specimen voids.

Principal conclusions from this study are (1) the methane reacts to form hydrogen, solid carbon, and traces of ethylene and acetylene; (2) a transition region of small temperature range exists below which the gas composition is frozen and above which the composition is in chemical equilibrium; (3) the transition region occurs at lower temperatures with greater carbon internal areas; (4) significant amounts of laminar-type carbon, not resulting from gas-phase reactions, were deposited in the specimen voids; and (5) the gas and solid temperatures apparently did not equilibrate until the gases approached the exit surface of the carbon.

INTRODUCTION

Charring ablator material has been found most effective as a thermal shielding material for a wide range of heating conditions associated with entry into planetary atmospheres. The effective performance of the charring ablator results primarily from a tough carbonaceous char layer which forms on the exterior surface of the material during heating and is capable of withstanding very high temperatures. Thus, during reentry a

significant amount of the total heat input at the surface is radiated to space by the high-temperature char surface. In addition, the gases generated in the pyrolysis zone of the charring ablator absorb energy by temperature increases and chemical reactions as they pass through the porous char layer.

The flow of pyrolysis gases through the hot char layer is one aspect of ablation about which relatively little is known. In particular, there is a lack of information concerning the extent of the chemical reactions that occur and the amount of energy absorbed by these reactions. Although much research has been done on the flow of fluids and gases through porous media in both the petroleum industry and the aerospace industry (for example, refs. 1 to 7), past studies have generally been restricted to nonreacting species, or frozen flow, which leads to the minimum absorption of energy. More recently, analytical ablation studies have assumed that the pyrolysis gases react to chemical equilibrium, which corresponds to the maximum absorption of energy (for example, ref. 8). Detailed analytical studies of finite-rate reactions of the pyrolysis gases have recently been completed (ref. 9) and limited experimental data on the flow of pyrolysis gases through chars at temperatures up to 2000° F (1370 K) have been obtained (ref. 10).

The primary objective of the study reported herein and in reference 11 was to provide experimental data on the thermal and chemical phenomena that occur during the flow of gases through porous matrices at very high temperatures. Resistance-heated porous carbon was used to simulate an ablative char. Methane, which is perhaps the most stable hydrocarbon product of ablator pyrolysis, was used as a pyrolysis gas with helium as the carrier gas to vary the methane mole fraction. Results which define the gas flow chemistry (i.e., frozen, reaction-kinetics controlled, or equilibrium) for temperatures up to 3800° R (2100 K) are given. In addition, a simplified analysis is used with test data to obtain estimates of the heat absorbed by the reaction of the gases as they pass through the porous carbon layer.

SYMBOLS

A	internal surface area per unit volume porous matrix
c_p	effective specific heat
d	mean pore diameter of porous matrix
H	total enthalpy of gas
H_o	total enthalpy at $T_g = 540^{\circ}$ R (300 K)

h	volumetric convective heat-transfer coefficient
k_s	effective conductivity of porous material
L	specimen thickness
$\dot{m}$	mass flow rate per unit area
p	gage pressure
Q_{CH_4}	total energy absorption by methane
q'	rate of heat generation per unit bulk volume
r	radial distance
T	temperature
T_g	gas temperature
$\overline{T}_g$	averaged gas temperature
$T_{g,max}$	maximum gas temperature
T_s	solid temperature
t	time
X_i	mole fraction, species i
x	axial distance from entrance surface
α	mass fraction
δ	deposition thickness
η	open-pore volume per unit volume (porosity)

Subscripts:

1 entrance surface

2 exit surface

The units used for the physical quantities defined in this paper are given both in U.S. Customary Units and in the International System of units (SI) (ref. 12). Appendix A presents factors relating these two systems of units.

EXPERIMENT

This program was undertaken to study the thermal and chemical phenomena occurring during flow of pyrolysis gases through the porous char layer of an ablation heat-shield material. For the experimental phase, resistance-heated porous-carbon specimens were used to simulate the porous char layer that is characteristic of charring ablators. The specimens were subjected to internal flow of methane, helium, and mixtures of methane and helium which simulated the pyrolysis-gas flow in ablation. Helium is not a pyrolysis gas but was used to vary the mole fraction of methane from one test to another.

Apparatus

Figures 1 and 2 are a photograph and a detailed schematic diagram of the test apparatus, which contains a heated porous-carbon slab. The carbon slab was heated by an electrical current introduced through the water-cooled terminals. Boron nitride insulation was bonded with porcelain cement to the carbon specimen and steel support plate. A gas plenum chamber was attached to the upstream support plate, and a quartz window was located in the end of this plenum chamber to permit monitoring of the temperature at the carbon inlet surface with an automatic pyrometer. The temperature at the carbon exit surface was similarly monitored with an automatic pyrometer. The test device was covered with a bell jar and was capable of operating for extended times with carbon surface temperatures over 4000° R (2200 K).

The gas flow (helium, methane, or a mixture of helium and methane) was metered to the test apparatus by a dual-float flowmeter. The inlet gas pressure and temperature (nominally room temperature) were determined by a pressure transducer and a thermocouple located in the plenum chamber as indicated. The test gases flowed through the porous carbon then exhausted into the bell jar (not shown) which was used to provide a controlled atmosphere. The test gases left the bell jar through pyrometer view ports.

A gas sampling device was located near the exit surface of the porous carbon. This device consisted of an evacuated gas sampling bottle to which a gas sampling tube was attached. The gas sampling tube entrance was located less than 1 inch (2 cm) from the downstream surface of the carbon.

Materials and Test Conditions

Test specimens of the form shown in figure 3 were machined from two grades of commercially available porous carbon, grades 25 and 45. Table 1 gives a summary of the properties of these materials. Specimen exit surface temperatures, specimen thicknesses, and gas flow rates are given in table 2.

Gases employed in this study were methane, helium, and mixtures of methane and helium. Methane was chosen as the hydrocarbon test gas because it is a simple hydrocarbon in terms of structure and because methane is a stable component of the identified gases leaving the pyrolysis zone of ablation materials (refs. 13 and 14).

Procedure

Test procedure.- The test apparatus was assembled with the desired specimen (grade and thickness) approximately 24 hours prior to conducting a test to assure complete curing of the porcelain cement.

Flow of nitrogen gas into the bell jar was begun several minutes before start of a test to purge the system of oxygen and to provide an inert atmosphere. Helium gas was metered through the porous specimen as electrical power was applied to the apparatus. The desired system temperature was obtained by adjusting the current flow in the apparatus. The system was permitted to remain at a given power level and helium flow rate for several minutes to assure that steady-state conditions existed. An indication of the stability of the system was obtained by monitoring the specimen surface temperatures, gas flow rate, and specimen current level.

After steady state was achieved, the gas flow through the specimen was switched from helium to the test gas, which was methane or a known mixture of methane and helium. Because of the different heat capacities of helium and the test gas plus any energy absorption due to chemical processes involving the test gas and the high-temperature porous specimen, the specimen temperature changed with introduction of the test gas. The system was permitted to remain at the initial power level with test gas flowing through the specimen until all temperatures and the gas flow were relatively steady. At this time, a gas sample was taken and the test terminated.

The magnitude of specimen temperature change resulting from change of gas flow from helium to the test gas depends upon the relative mass flow rate and the specific heats of helium and the test gas. By proper selection of helium and test-gas flow rates, this

change in thermal-equilibrium temperature of the system with flow change was reduced sufficiently for steady-state conditions with test gas flow to be achieved in a reasonable time (generally 120 sec).

Data recorded during each test included specimen surface temperature history, gas temperature and upstream gas pressure histories, and gas flow rate.

Gas analysis procedure.- Gas samples collected during each test were analyzed with a mass spectrometer. In general, each gas sample was scanned over a range of mass-charge ratio from 2 to 44 corresponding to species ranging in mass number from 2 for hydrogen to 44 for carbon dioxide. At the outset of this program, a number of gas samples were scanned to higher values of mass-charge ratio in search of other species, but no evidence of species with a mass-charge ratio higher than 44 was found.

Porous-specimen analysis procedure.- Post-test analyses were made on several of the porous-carbon specimens by metallographic techniques, which permitted observation of the microstructure of the specimens before and after testing. In preparing a sample for metallographic analysis, it was vacuum impregnated with a room-temperature-curing epoxy resin selected for its viscosity and surface tension. This process penetrated the open-pore network with a clear, bubble-free, hard filler, which permitted polishing of the porous specimens by standard metallurgical methods. After the specimens were impregnated, they were sectioned so that cross sections through the thickness of the specimens were obtained. These sections were polished and viewed and/or photographed with a metallograph at magnifications ranging from $\times 50$ to $\times 1000$. Measurements of carbon deposition thickness were made with a filar micrometer stage in the metallograph.

Porosity data were obtained for both grades of specimen material before testing and for a limited number of post-test specimens with a mercury-intrusion porosimeter. This instrument gives a pore spectrum of all open voids from 0.002 to 100 microns (micrometers) in diameter.

ANALYSIS

Treatment of the exact problem of reacting gas flow through a porous matrix is not possible at this time. Much of the difficulty of the problem stems from the complexity of the chemistry of hydrocarbon gas flow through a high-temperature porous matrix. A simplified analytical model (derived and discussed in ref. 11) is used herein in order to provide insight into the experimental results.

The differential equations describing steady, one-dimensional constant-property flow of gas through a resistance-heated porous matrix neglecting diffusion are

$$k_s \frac{d^2T_s}{dx^2} + q' = h\left(T_s - T_g\right)$$

$$\dot{m} c_p \frac{dT_g}{dx} = h\left(T_s - T_g\right)$$

Although the conductivity of the solid is temperature dependent, it was assumed to be constant for a given case and evaluated at the temperature of the exit surface which was used as a representative temperature of the solid. To account for energy absorption by chemical reactions, an effective specific heat was defined as

$$c_p = \frac{H - H_o}{\overline{T}_g}$$

where

$$\overline{T}_g = \frac{1}{L} \int_0^L T_g(x)dx$$

The differential equations were solved to obtain algebraic equations for T_s and T_g as a function of x. These equations were then used to determine the gas and solid temperature profiles through the specimen for each test in this study. These computed data were employed in analysis of the experimental data.

It should be stressed that the differential equations are severely restricted because of the assumptions made to obtain a solution. The most restrictive assumption was that of constant properties. Employing a constant-mean specific heat has the effect of spreading the energy absorption processes due to endothermic chemical reactions uniformly throughout the specimen. It is felt that calculations made with a constant effective specific heat provide a good description of the total system; however, the local processes are less accurately described.

RESULTS AND DISCUSSIONS

Table 2 presents a summary of data obtained in this program. Section I of table 2 gives the preexposure data for each test point. Section II outlines the experimental conditions under which the test was conducted. Section III contains results of mass spectrometric analysis of the gas samples collected in the course of the experimental tests. The mass analysis data for the combined gas and solid phases were computed from the initial gas composition and the final test gas composition, where conservation of carbon and hydrogen is imposed. Section IV contains results from the computations made for each test point.

Typical Results

Figure 4 shows pressure and temperature histories for a typical test. The data here are for test 9. The test specimen was grade 25 porous carbon, 0.025 ft (0.76 cm) thick. The test gas was pure methane flowing at a rate of 0.039 lbm/ft^2-sec (0.19 kg/m^2-s). For the period from 0 to 12 seconds, helium flowed through the specimen. During this time, the specimen was brought to the desired temperature level. At 12 seconds, the flow was switched from helium to methane. Note the drop in pressure and temperature. The drop in temperature results from the increased energy absorption by the test gas; the drop in pressure results from a combination of viscosity and density differences between helium and test gas flow. Steady-state conditions are indicated by the fact that temperature and pressure remain constant. Steady-state conditions for the system were reached after about 50 seconds. The test gas sample was taken at 87 seconds, and the test gas flow was changed to helium flow at 110 seconds. Analysis of the gas sample showed the test gas (methane) to have degraded to 0.84 mole CH_4, 0.008 mole C_2H_2, and 0.156 mole H_2. The amount of condensed carbon was determined by conservation of the species carbon, which could not be observed by gas analysis. Indications are that some of the carbon formed by decomposition of hydrocarbon gases is deposited in the specimen.

The experimental data of figure 4 were used with the solutions of the differential equations to compute the temperature profiles existing in the system at the time the gas sample was taken. Figure 5, which shows the results of those computations, indicates that the test gas leaves the specimen at essentially the exit surface temperature; this was found to be true for all tests. However, the salient feature of figure 5 is the slow response of the gas temperature to the heat-transfer potential $(T_s - T_g)$. At $x/L = 0.50$, the solid and gas temperatures still differ by 200° R (110 K) although the heat-transfer potential to that point has been large.

The significance of this temperature differential is better understood when the properties of the porous carbon are compared with those of typical ablation chars. Because chars are typically twice as porous and permeable as the carbon specimens (refs. 15, 16, and 17), there is likely to be less thermal contact between gas and solid surfaces in a char than in the carbon of the present investigation. Larger gas-solid temperature differences therefore may be expected in an ablator char layer.

Chemical Reactions and Energy Absorption

Figure 6 presents the equilibrium chemical composition as a function of temperature for methane at a pressure of 1 atmosphere. These data were computed with a program based on minimization of the free energy (ref. 18).

Methane is seen to begin significant degradation at about 750° R (420 K). From about 1000° to 1500° R (600 to 850 K) the equilibrium mole fraction of methane diminishes sharply. At 2000° R (1100 K) the methane mole fraction in the mixture is only about 0.02, and at 2500° R (1400 K) and above only traces of methane are computed. The products of methane degradation are hydrogen and solid carbon at temperatures up to 1800° R (1000 K). Traces of ethylene and acetylene are predicted at temperatures above 1800° R (1000 K) with acetylene becoming more noticeable near 5000° R (2800 K).

The mass spectrometric technique used to analyze the gas sample taken at the exit surface is not capable of detecting solid carbon. Thus, only the gaseous species will be detected. Furthermore, if the gas temperatures are in the range of primary concern from 2500° to 4000° R (1400 to 2200 K) and chemical equilibrium exists, the only gas present will be hydrogen with a mole fraction of 1.0. On the other hand, if the methane does not decompose (frozen composition), the hydrogen mole fraction of the sample will be 0. Thus, the hydrogen mole fraction is a convenient index of the extent to which the methane reacts.

Figure 7 presents chemical analysis data for all the tests conducted in this program for the two grades of porous carbon. The hydrogen mole fraction is shown as a function of the measured exit surface temperature, which was chosen as representative of the solid temperature profile. Although the data shown are from tests with different initial mole fractions of methane, mass flow rates, and thicknesses of carbon, a single faired curve gives a good correlation between hydrogen mole fraction and exit surface temperature. Since exit surface temperature is essentially the same as the calculated maximum gas temperature, this suggests that the maximum gas temperature is a principal parameter in the reaction process.

Very little hydrogen is indicated at temperatures near the lower end of the abscissa. As the temperature increases, hydrogen concentration increases, undergoing a large increase over a narrow temperature band, then at higher temperatures changing more slowly to a value of 1.0 which corresponds to the equilibrium-theory calculation.

For purposes of discussion, the curves in figure 7 may be segmented, somewhat arbitrarily, into three parts. That region where little hydrogen is indicated may be termed "frozen composition" since the chemical reactions are very nearly frozen. The region of high hydrogen concentration is labeled equilibrium composition since the composition is near chemical equilibrium. The intermediate region is a transition region where the chemical composition is largely controlled by reaction kinetics. The transition region leads to the concept of a transition temperature which may be defined as the gas temperature at which the rate of change of hydrogen concentration with temperature is greatest. Even in this preliminary form, the concept of a transition temperature can be used in analytical studies of ablation (ref. 19).

Figure 7 shows a difference in the transition temperature for the two grades of porous carbon. Figure 7(a) shows a transition temperature near 2900° R (1610 K) for grade 25 porous carbon whereas figure 7(b) shows a transition temperature near 2650° R (1470 K) for grade 45. In an attempt to understand the difference in transition temperature indicated by figure 7, the mean pore diameter of the materials (table 1) used in simulating the ablator char layer was examined.

The internal surface area of a porous material is greatly affected by its characteristic dimension, or mean pore diameter. To estimate the relation between internal surface area of the two grades of materials, it is assumed that each material consists of a solid phase containing interconnected spherical voids of diameter listed in table 1. The internal surface area per unit volume for such a structure is given by

$$A = \frac{6\eta}{d}$$

From this expression, the surface area of grade 45 porous carbon was found to be twice that of grade 25.

The effect of variation of internal surface area on a chemically reacting flow through a porous medium may be explained as follows: Considering the chemical processes as involving an inelastic collision between reactants, products, and the wall of the flow channel will provide an explanation of the importance of surface area on the performance of the system. When the temperature of the porous solid (and the internal surface) is much higher than that of the gaseous molecules, a collision of a gas molecule with the wall of the flow channel is more likely to result in transfer of sufficient energy to bring about a chemical reaction than is a collision of two gas molecules. Grade 45 porous carbon has nearly twice the surface area of grade 25; hence collisions between gas molecules and the wall are much more prevalent for grade 45 than for grade 25. Therefore, in a given situation more hydrogen would be present in flow from a grade 45 specimen than from a grade 25 specimen, or in terms of transition temperature, grade 45 porous carbon should exhibit a lower transition temperature than grade 25 porous carbon.

Although many mechanisms are given in the literature for the pyrolysis of methane, the scheme proposed by reference 20 is of particular interest. That scheme involves the following reactions:

$$2CH_4 \rightarrow C_2H_6 + H_2$$

$$C_2H_6 \rightarrow C_2H_4 + H_2$$

$$C_2H_4 \rightarrow C_2H_2 + H_2$$

which explain the presence of hydrogen, acetylene, and ethylene in the tests reported herein. The proposed reaction consuming ethane is faster than the reaction forming this compound; hence no ethane is expected in the products. A simultaneous polymerization and dehydrogenation process involving acetylene is suggested in reference 20 as the final step of the series producing solid carbon. The presence of solid carbon as a pyrolysis product of methane was observed in this investigation and will be discussed subsequently.

Figure 8 shows computed energy absorption data for methane as a function of the measured surface temperature at the specimen exit. This quantity is defined as the total enthalpy of the products of pyrolysis and any unreacted methane, at the temperature computed for the gas at the exit surface, less the total enthalpy of methane at the temperature of the flow entering the system (540° R (300 K)). Results for equilibrium and frozen conditions are included for comparison. The data show that at the high exit surface temperatures, the energy absorbed by chemical reactions may be as much as 2000 Btu/lbm (4.6 MJ/kg) of methane introduced. In addition, these figures show the same trends in the data as did figure 7, that is, the near-frozen-flow region, near-equilibrium-flow region, and the transition region, where the composition changes from frozen to equilibrium flow.

Carbon Deposition in the Simulated Char

As indicated previously, carbon deposition occurred in the porous carbon specimens during some of the tests. Figure 9 contains typical photomicrographs of the two grades of porous carbon before and after testing. Void areas and carbon areas are pointed out in the preexposure photomicrographs for reference purposes. In the postexposure photomicrographs, the lighter areas bordering the carbon areas are carbon deposited from the test gas flow.

Figure 10 is a photomicrograph of grade 25 porous carbon (under polarized light) showing a more detailed view of the character of the carbon deposited during flow of the methane-helium mixture through the specimen. The obvious laminar-type structure of the carbon deposit results from pyrolytic deposition of carbon atoms layer by layer on the porous-carbon grain. Note the pronounced growth cones and the undulating surface of the deposit which result from the roughness of the porous-carbon grains. It is also of interest that the thickness of deposition seems to be uniform over the walls of a void and smaller regions are thus completely filled. (See the lower right portion of the void.) In terms of the total specimen, this means that smaller pores are filled before larger pores.

In order to determine how the carbon deposition varied in the direction of the gas flow, a sequence of measurements of deposition thickness at known depths in a specimen (test 2) after exposure to the test gas flow was made. The carbon deposition thicknesses

were measured with a metallograph having a lens with a built-in scale. The measured thicknesses are related to axial position in the specimen in figure 11, which also shows computed gas and solid temperatures. The deposition thickness is large at the specimen entrance surface and builds up to a maximum value in a very short distance. Thereafter, the thickness decreases until there is no discernible amount near the exit surface.

Measurements of the carbon deposition thickness in the radial direction (normal to the gas flow direction) were also made by metallographic means and are given in figure 12. The measurements were made at $x/L = 1/4$ in the test specimen; this axial location is just downstream of the point of maximum axial deposition thickness. Although there is some scatter in the measurement data, there is an apparent decrease in deposition thickness in the radial direction from the specimen axis. However, in the region r/L less than 1, the decrease is not severe and the deposition process was treated as one dimensional.

An explanation of the formation of carbon deposits can be found in reference 21 which reports on a study of the decomposition of cool hydrocarbon gases by vapor deposition in the presence of a high-temperature surface. In that study when methane was passed over a heated rod, a highly oriented, laminar-type carbon deposit, such as that shown in figure 10 was formed. Reference 21 concludes that the rate of vapor deposition is determined primarily by the effective collision rate at the hot surface. However, if the gas temperature is sufficiently high, the production of carbon by gas-phase reactions will reduce the amount of vapor deposition.

The vapor deposition of carbon was not detected in all the tests identified in table 2. Test 5 is an example for which no evidence of vapor-deposited carbon was detected in the postexposure metallographic analysis of the specimen. However, carbon was obviously produced by the gas-phase reactions as indicated by the large mole fraction of hydrogen in the test gas sample. Some carbon in the form of soot was observed on the specimen electrical insulator and quite likely some amorphous carbon was deposited in the specimen which would be indistinguishable from the grain of the porous-carbon matrix.

Porosity Data

The porosities of specimens of porous carbon were determined by the mercury-intrusion technique before testing. The porosity η of grades 25 and 45 porous carbon was found to be 0.47 for both. Typical distributions of the pore sizes are given in figure 13 for bands of pore diameters. The average pore diameter (defined as the sum of the products of the band average diameter and band porosity fraction) was found to be 119 μm and 64 μm for grades 25 and 45, respectively.

After exposure, the specimen of test 2 was cut in half to determine the porosity for the regions from $x/L = 0$ to 0.5 and $x/L = 0.5$ to 1. The porosity was 0.32 for the former region and 0.45 for the latter region. The pore-size distributions are given in figure 14.

The porosity decrease from 0.47 to 0.32 in the region $0 < x/L < 0.5$ is attributed to vapor deposition of carbon. Figure 14(a) indicates an increase in smaller pore sizes after exposure which results in a smaller average pore diameter (98 μm) than for the untested specimen of figure 13(a). On the other hand, the postexposure porosity (0.45) of the region $0.5 < x/L < 1.0$ is about the same as that for the untested specimen (0.47), as is the distribution of pore sizes (fig. 14(b)).

CONCLUDING REMARKS

Information on the thermochemical reactions that occur during the flow of pyrolysis gases through the char layer of an ablator is difficult to obtain from controlled experiments. This situation exists because of the complexity of the pyrolysis-gas reactions and the fact that the char internal temperature distributions cannot be duplicated.

In order to obtain qualitative data related to the complex ablation process, an idealized model was used to simulate the ablator. Mixtures of methane and helium, which simulated pyrolysis gases, were passed through resistance-heated porous carbon specimens, which simulated the hot char layer. Carbon of two different porosities was tested with various flow rates, methane concentrations, specimen thicknesses, and a range of maximum specimen temperatures up to about 3800° R (2100 K). Temperature differences across the carbon specimens of 400° to 800° R (200 to 400 K) were obtained by varying the gas flow rates.

The principal results from the series of tests are

1. Methane pyrolyzed to form hydrogen and solid carbon with traces of ethylene and acetylene.

2. The hydrogen mole fraction in the effluent gas mixture was correlated with the temperature at the carbon specimen exit surface to define a narrow transition temperature region below which the gas flow was nearly chemically frozen and above which, nearly in chemical equilibrium. In the transition region, the chemical composition of the gases is expected to be controlled by reaction kinetics.

3. The transition region occurred at lower temperatures for the carbon layer having the greater internal surface area.

4. Significant depositions of laminar-type carbon occurred in the voids of the porous carbon matrices. The maximum deposition existed in a region near the specimen entrance surface.

5. As expected, computed gas temperatures lag the solid carbon temperatures near the entrance surface. However, this state of thermal nonequilibrium apparently persisted well into the porous carbon and the gas temperature did not reach the solid temperature

until the exit surface was approached. This suggests that the usual assumption of thermal equilibrium between a gas and a porous solid through which the gas is flowing needs further study.

Langley Research Center,
National Aeronautics and Space Administration,
Langley Station, Hampton, Va., June 25, 1969.

APPENDIX A

CONVERSION OF U.S. CUSTOMARY UNITS TO SI UNITS

The International System of Units (SI) (ref. 12) was adopted in 1960 by the Eleventh General Conference on Weights and Measures held in Paris, France. Conversion factors required for the base units and the derived units used herein are given in the following table:

Physical quantity	U.S. Customary Unit	Conversion factor (*)	SI unit
Area	ft^2	0.093	meters^2 (m^2)
Density	lbm/ft^3	16.02	kilograms/meter^3 (kg/m^3)
Energy	Btu	1055	joules (J)
Thermal efficiency	Btu/lbm	2.326×10^3	joules/kilogram (J/kg)
Force	lbf	4.448	newton (N)
Length	ft	0.305	meter (m)
	in.	0.0254	meter (m)
Mass	lbm	0.454	kilogram (kg)
Pressure	lbf/ft^2	47.88	newtons/meter^2 (N/m^2)
	lbf/in^2	6.895×10^3	newtons/meter^2 (N/m^2)
	atm	1.013×10^5	newtons/meter^2 (N/m^2)
Thermodynamic	^oR	5/9	kelvin (K)

*Multiply value given in U.S. Customary Units by conversion factor to obtain equivalent value in SI units.

Prefixes to indicate multiples of units are as follows:

Prefix	Multiple
micro (μ)	10^{-6}
centi (c)	10^{-2}
kilo (k)	10^3
mega (M)	10^6

REFERENCES

1. Jenkins, R.; and Aronofsky, J. S.: Analysis of Heat Transfer Processes in Porous Media – New Concepts in Reservoir Heat Engineering. Miner. Ind. Exp. Sta. Bull. No. 64, Pennsylvania State Univ., 1954, pp. 69-74.

2. Green, Don W.; and Perry, Robert H.: Heat Transfer With a Flowing Fluid Through Porous Media. Chem. Eng. Progr. Symp. Ser., no. 32, vol. 57, 1961, pp. 61-68.

3. Preston, Floyd W.: Mechanism of Heat Transfer in Unconsolidated Porous Media at Low Flow Rates. Ph. D. Thesis, Pennsylvania State Univ., 1957.

4. Koh, J. C. Y.; and Del Casal, E.: Heat and Mass Flow Through Porous Matrices for Transpiration Cooling. Proceedings of the 1965 Heat Transfer and Fluid Mechanics Institute, Andrew F. Charwat, ed., Stanford University Press, c.1965, pp. 263-281.

5. Bland, D. R.: Mathematical Theory of the Flow of a Gas in a Porous Solid and of the Associated Temperature Distributions. Proc. Roy. Soc. (London), ser. A, vol. 221, no. 1144, Jan. 7, 1954, pp. 1-28.

6. Grootenhuis, P.: The Mechanism and Application of Effusion Cooling. J. Roy. Aeronaut. Soc., vol. 63, no. 578, Feb. 1959, pp. 73-89.

7. Koh, J. C. Y.; and Del Casal, E. P.: Heat and Mass Transfer With Chemical Reactions for Fluid Flow Through a Porous Matrix in Re-Entry Thermal Protection. AIAA Paper No. 66-423, June 1966.

8. Kratsch, K. M.; Hearne, L. F.; and McChesney, H. R.: Thermal Performance of Heat Shield Composites During Planetary Entry. Paper presented at AIAA-NASA National Meeting (Palo Alto, Calif.), Sept. 30 – Oct. 1, 1963.

9. Del Valle, E. G.; April, G. C.; and Pike, R. W.: Modeling for a Set of Complex Chemical Reactions at High Temperature. Preprint 8F, Amer. Inst. Chem. Eng., Dec. 1968.

10. April, Gary C.; Pike, Ralph W.; and Del Valle, Eduardo G.: Experimental Verification of the Non-Equilibrium Model for Predicting Behavior in the Char Zone of a Charring Ablator – Evaluation of the Energy Transfer in the Char Zone During Ablation. NASA CR-66646, 1968.

11. Clark, Ronald K.: Flow of Hydrocarbon Gases in Porous Media at Elevated Temperatures. M.A.E. Thesis, Univ. of Virginia, Aug. 1968.

12. Comm. on Metric Pract.: ASTM Metric Practice Guide. NBS Handbook 102, U.S. Dep. Com., Mar. 10, 1967.

13. Sykes, George F., Jr.: Decomposition Characteristics of a Char-Forming Phenolic Polymer Used for Ablative Composites. NASA TN D-3810, 1967.

14. Sykes, George F.; and Nelson, James B.: Thermoanalysis of Ablation Materials. Paper presented at American Institute of Chemical Engineers Meeting (Houston, Tex.), Feb. 1967.

15. Wilson, R. Gale, compiler: Thermophysical Properties of Six Charring Ablators From 140° to 700° K and Two Chars From 800° to 3000° K. NASA TN D-2991, 1965.

16. Pyron, C. M., Jr.; and Pears, C. D.: The Permeabilities of Three Porous Graphites. Rep. 8059-1728-2-III (Contract NAS 1-5448), Southern Res. Inst., Oct. 11, 1966.

17. Engelke, W. T.; Pyron, C. M., Jr.; and Pears, C. D.: Thermophysical Properties of a Low-Density Phenolic-Nylon Ablation Material. NASA CR-809, 1967.

18. Stroud, C. W.; and Brinkley, Kay L.: Chemical Equilibrium of Ablation Materials Including Condensed Species. NASA TN D-5391, 1969.

19. Brewer, William D.; Stroud, C. W.; and Clark, Ronald K.: Effect of the Chemical State of Pyrolysis Gases on Heat-Shield Mass. NASA TN D-4975, 1968.

20. Porter, George: The Mechanism of Carbon Formation. AGARD Mem. AG13/M9, [1954].

21. Carley-Macauly, K. W.; and Mackenzie, M.: Studies on the Deposition of Pyrolytic Carbons. Proceedings of the Fifth Conference on Carbon, Vol. 2, Macmillan Co., 1963, pp. 449-459.

TABLE 1.- PHYSICAL PROPERTY DATA FOR POROUS CARBON

Grade	Density (a)		Porosity	Mean pore diameter (b)		Permeability (c)	
	lbm/ft^3	kg/m^3	(b)	ft	μm	ft^2/min	cm^2/s
25	64.4	1032	0.47	0.00039	119	5.29	2500
45	65	1042	.47	.00019	58	2.75	1300

[a]From manufacturer's literature.

[b]Measured.

[c]Measured at room temperature with helium (ref. 16).

TABLE 2.- SUMMARY OF TEST DATA FOR SIMULATION OF PYROLYSIS-GAS FLOW THROUGH A CHAR LAYER

[Initial gas temperature, 540° R]

(a) U.S. Customary Units

I – Preexposure data					II – Experimental conditions					III – Final test gas composition										IV – Analytical computation results		
Test	Material grade	Specimen thickness, ft	Test gas		Gas flow rate, lbm/ft^2-sec	Upstream pressure, lbf/ft^2	Test time, sec	$T_{s,1}$, °R	$T_{s,2}$, °R	Gas phase – mole basis (CH_4)				Gas and solid phases – mass basis (CH_4 and He)						$T_{g,max}$, °R	$T_{g,2}$, °R	Q_{CH_4}, Btu/lbm
			X_{CH_4}	X_{He}						X_{CH_4}	$X_{C_2H_2}$	$X_{C_2H_4}$	X_{H_2}	α_{CH_4}	$\alpha_{C_2H_2}$	$\alpha_{C_2H_4}$	α_{H_2}	$\alpha_{C(s)}$	α_{He}			
1	25	0.0333	1.0000	0	0.0324	216	30	3314	3815	0.005	0.005	(a)	0.990	0.010	0.017	(a)	0.248	0.725	0	3912	3907	6273
2	25	.0333	1.0000	0	.0330	176	30	3188	3715	(a)	(a)	(a)	1.0	(a)	(a)	(a)	.250	.750	0	3800	3796	6054
3	25	.0333	.2583	.7417	.0368	422	75	3152	3560	.010	.008	(a)	.982	.012	.015	(a)	.141	.414	.418	3503	3503	5688
4	25	.0333	.0903	.9097	.0366	393	60	3087	3633	.030	(a)	(a)	.970	.017	(a)	(a)	.067	.201	.715	3830	3794	5906
5	25	.0333	.2583	.7417	.0668	378	105	2399	3165	.093	(a)	(a)	.907	.099	(a)	(a)	.121	.362	.418	3076	3076	4658
6	25	.025	.2583	.7417	.0652	180	195	2155	2994	.123	(a)	(a)	.877	.128	(a)	(a)	.114	.340	.418	2970	2970	4393
7	25	.025	.2583	.7417	.0368	101	60	2218	2895	.539	.021	0.014	.426	.404	.027	0.018	.040	.093	.418	2980	2958	3397
8	25	.025	.2583	.7417	.0367	114	105	2208	2698	.876	.011	(a)	.112	.543	.011	(a)	.008	.019	.418	2753	2745	2396
9	25	.025	1.0000	0	.0390	16	75	2093	2635	.840	.008	(a)	.156	.910	.014	(a)	.021	.055	0	2696	2683	2363
10	25	.025	.2583	.7417	.0688	246	90	2141	2970	.488	.069	(a)	.453	.379	.087	(a)	.044	.072	.418	2956	2956	3859
11	25	.025	.1244	.8756	.0297	(b)	72	(c)	2887	.525	.034	(a)	.441	.250	.026	(a)	.026	.061	.637	(d)	(d)	(d)
12	25	.025	.1244	.8756	.0401	(b)	45	2337	2895	.288	.016	(a)	.696	.162	.015	(a)	.049	.137	.637	2927	2925	3920
13	25	.025	.1244	.8756	.0353	(b)	60	2191	2780	.767	.017	(a)	.216	.316	.011	(a)	.011	.025	.637	2864	2839	2732
14	25	.025	.2583	.7417	.0178	(b)	55	(c)	2818	.140	.078	(a)	.782	.146	.130	(a)	.100	.209	.418	(d)	(d)	(d)
15	45	.0208	1.0000	0	.0327	302	15	3230	3820	(a)	.007	(a)	.993	(a)	.023	(a)	.248	.729	0	3990	3960	6373
16	45	.0333	1.0000	0	.0327	164	25	2225	2780	.262	.034	.013	.693	.410	.086	.035	.136	.333	0	2712	2712	3910
17	45	.0333	.2583	.7417	.0376	284	30	2213	2655	.667	(a)	(a)	.333	.466	(a)	(a)	.029	.086	.418	2636	2636	2522
18	45	.0333	.2583	.7417	.0642	1045	72	2535	3253	.068	(a)	(a)	.932	.074	(a)	(a)	.127	.380	.418	3130	3130	4835
19	45	.0333	1.0000	0	.0353	142	116	2122	2670	.281	(a)	(a)	.719	.439	(a)	(a)	.140	.421	0	2607	2607	3367
20	45	.0333	.1244	.8756	.0407	734	120	1885	2576	.930	(a)	(a)	.070	.562	(a)	(a)	.005	.015	0	2660	2645	2128

[a]Trace of this species detected.

[b]No upstream pressure data available.

[c]No entrance surface temperature data available.

[d]Computations not possible because of lack of entrance surface temperature data.

TABLE 2.- SUMMARY OF TEST DATA FOR SIMULATION OF PYROLYSIS-GAS FLOW THROUGH A CHAR LAYER – Concluded

[Initial gas temperature, 300 K]

(b) SI Units

I – Preexposure					II – Experimental conditions					III – Final test gas composition											IV – Analytical computation results		
Test	Material grade	Specimen thickness, cm	Test gas		Gas flow rate, kg/m^2-s	Upstream pressure, kN/m^2	Test time, sec	$T_{s,1}$, K	$T_{s,2}$, K	Gas phase – mole basis (CH_4)					Gas and solid phases – mass basis (CH_4 and He)						$T_{g,max}$, K	$T_{g,2}$, K	Q_{CH_4}, MJ/kg
			X_{CH_4}	X_{He}						X_{CH_4}	$X_{C_2H_2}$	$X_{C_2H_4}$	X_{H_2}	α_{CH_4}	$\alpha_{C_2H_2}$	$\alpha_{C_2H_4}$	α_{H_2}	$\alpha_{C(s)}$	α_{He}			
1	25	1.015	1.0000	0	0.158	10.34	30	1840	2120	0.005	0.005	(a)	0.990	0.010	0.017	(a)	0.248	0.725	0	2179	2176	14.60
2	25	1.015	1.0000	0	.161	8.43	30	1770	2061	(a)	(a)	(a)	1.0	(a)	(a)	(a)	.250	.750	0	2111	2109	14.12
3	25	1.015	.2583	.7417	.180	20.20	75	1750	1978	.010	.008	(a)	.982	.012	.015	(a)	.141	.414	.418	1944	1944	13.25
4	25	1.015	.0903	.9097	.179	18.82	60	1715	2019	.030	(a)	(a)	.970	.017	(a)	(a)	.067	.201	.715	2125	2108	13.78
5	25	1.015	.2583	.7417	.326	18.20	105	1332	1758	.093	(a)	(a)	.907	.099	(a)	(a)	.121	.362	.418	1708	1708	10.87
6	25	.762	.2583	.7417	.318	8.62	195	1195	1663	.123	(a)	(a)	.877	.128	(a)	(a)	.114	.340	.418	1650	1650	10.23
7	25	.762	.2583	.7417	.180	4.84	60	1231	1609	.539	.021	0.014	.426	.404	.027	0.018	.040	.093	.414	1656	1643	7.92
8	25	.762	.2583	.7417	.179	5.46	105	1226	1499	.876	.011	(a)	.112	.543	.011	(a)	.008	.019	.418	1529	1525	5.58
9	25	.762	1.0000	0	.190	.77	75	1162	1463	.840	.008	(a)	.156	.910	.014	(a)	.021	.055	0	1496	1492	5.50
10	25	.762	.2583	.7417	.336	11.80	90	1190	1649	.488	.069	(a)	.453	.379	.087	(a)	.044	.072	.418	1641	1641	8.99
11	25	.762	.1244	.8756	.145	(b)	72	(c)	1603	.525	.034	(a)	.441	.250	.026	(a)	.026	.061	.637	(d)	(d)	(d)
12	25	.762	.1244	.8756	.196	(b)	45	1297	1609	.288	.016	(a)	.696	.162	.015	(a)	.049	.137	.637	1625	1624	9.14
13	25	.762	.1244	.8756	.172	(b)	60	1218	1545	.767	.017	(a)	.216	.316	.011	(a)	.011	.025	.637	1592	1577	6.37
14	25	.762	.2583	.7417	.087	(b)	55	(c)	1565	.140	.078	(a)	.782	.146	.130	(a)	.100	.209	.418	(d)	(d)	(d)
15	45	.634	1.0000	0	.160	14.48	15	1792	2122	(a)	.007	(a)	.993	(a)	.023	(a)	.248	.729	0	2218	2188	14.82
16	45	1.015	1.0000	0	.160	7.86	25	1235	1545	.262	.034	.013	.693	.410	.086	.035	.136	.333	0	1512	1512	9.12
17	45	1.015	.2583	.7417	.184	13.61	30	1228	1473	.667	(a)	(a)	.333	.466	(a)	(a)	.029	.086	.418	1463	1463	5.87
18	45	1.015	.2583	.7417	.314	50.10	72	1409	1805	.068	(a)	(a)	.932	.074	(a)	(a)	.127	.380	.418	1739	1739	11.24
19	45	1.015	1.0000	0	.172	6.8	116	1179	1483	.281	(a)	(a)	.719	.439	(a)	(a)	.140	.421	0	1449	1449	7.85
20	45	1.015	.1244	.8756	.198	35.16	120	1048	1429	.930	(a)	(a)	.070	.562	(a)	(a)	.005	.015	0	1477	1470	4.96

[a]Trace of this species detected.

[b]No upstream pressure data available.

[c]No entrance surface temperature data available.

[d]Computations not possible because of lack of entrance surface temperature data.

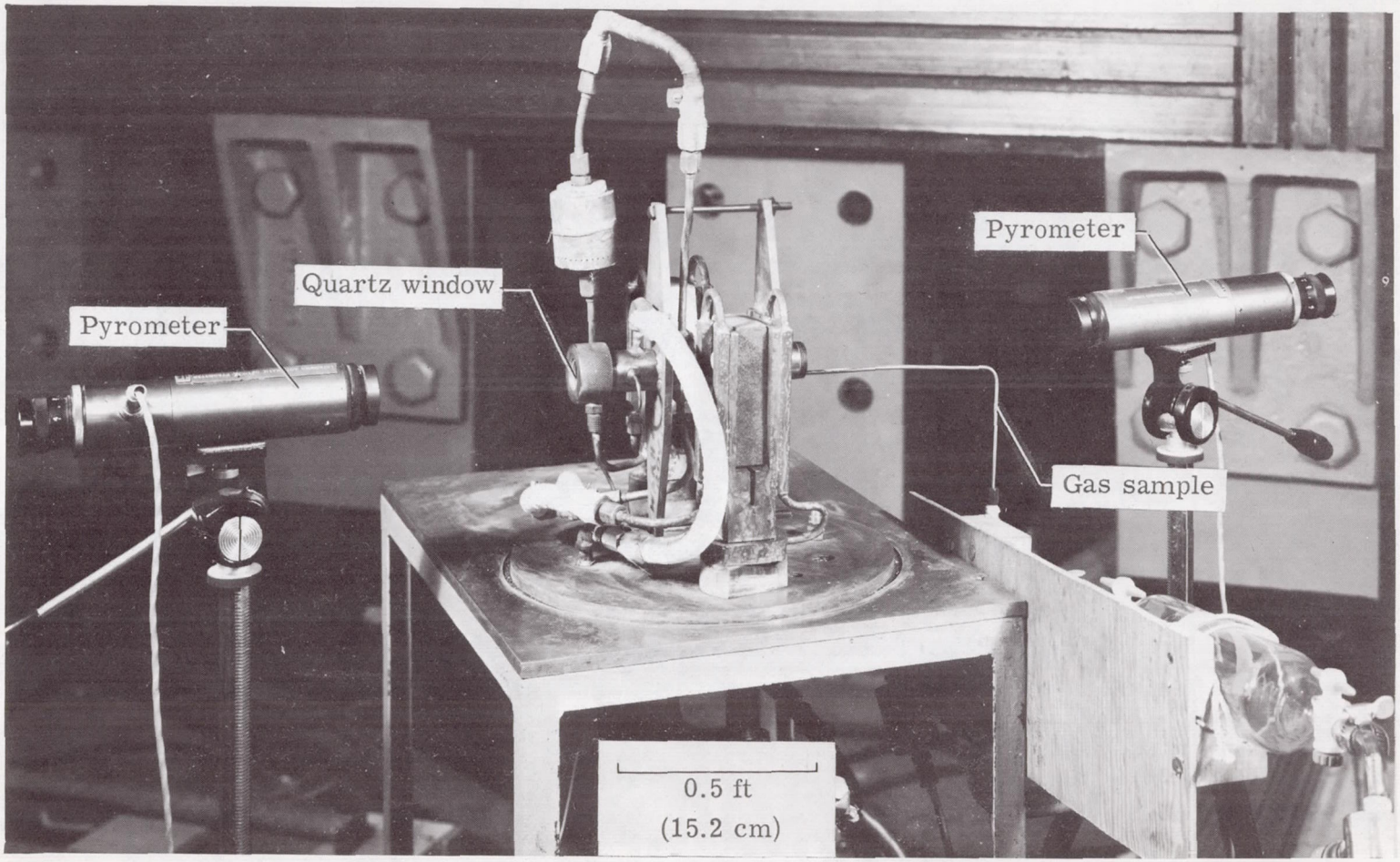

Figure 1.- Photograph of test apparatus. L-69-5255

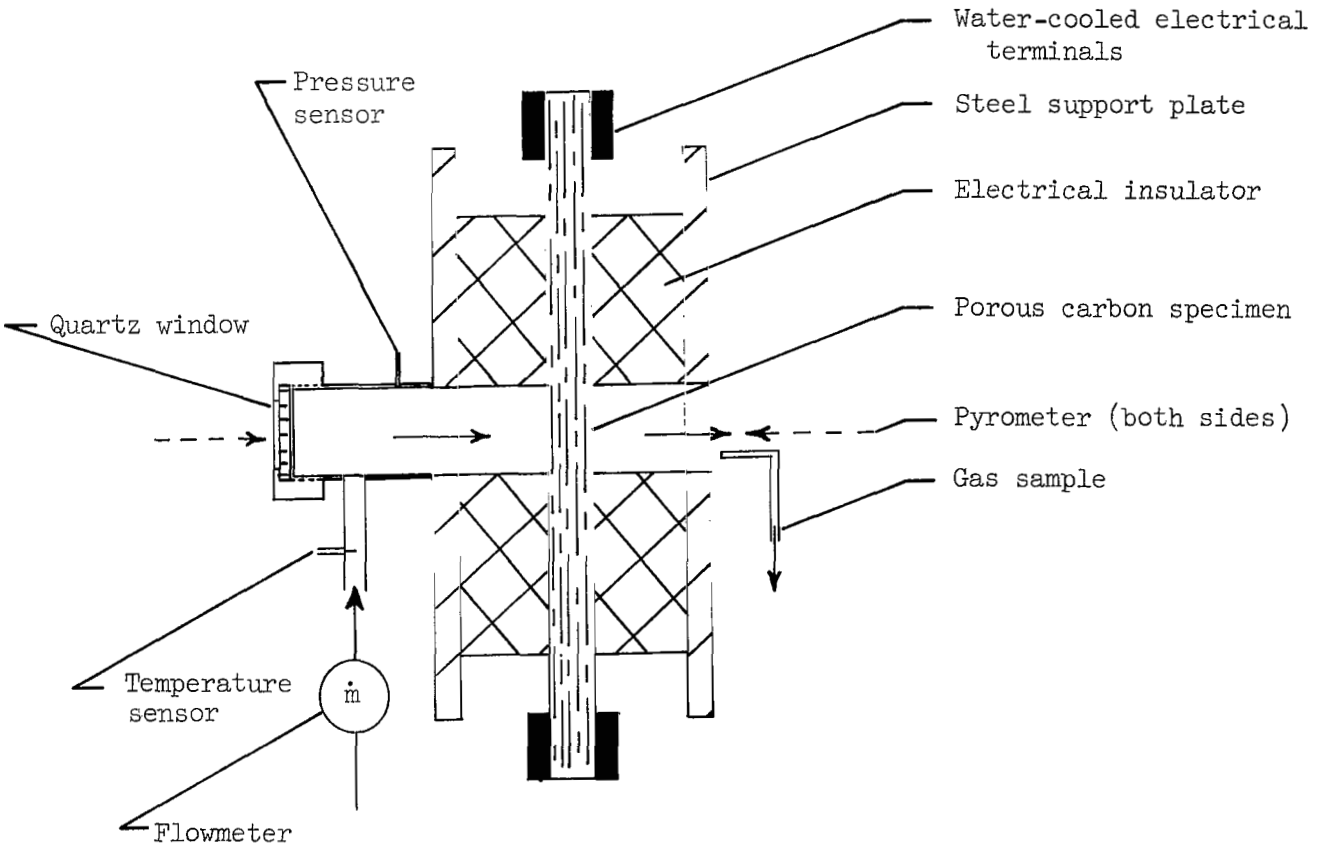

Figure 2.- Schematic diagram of test apparatus.

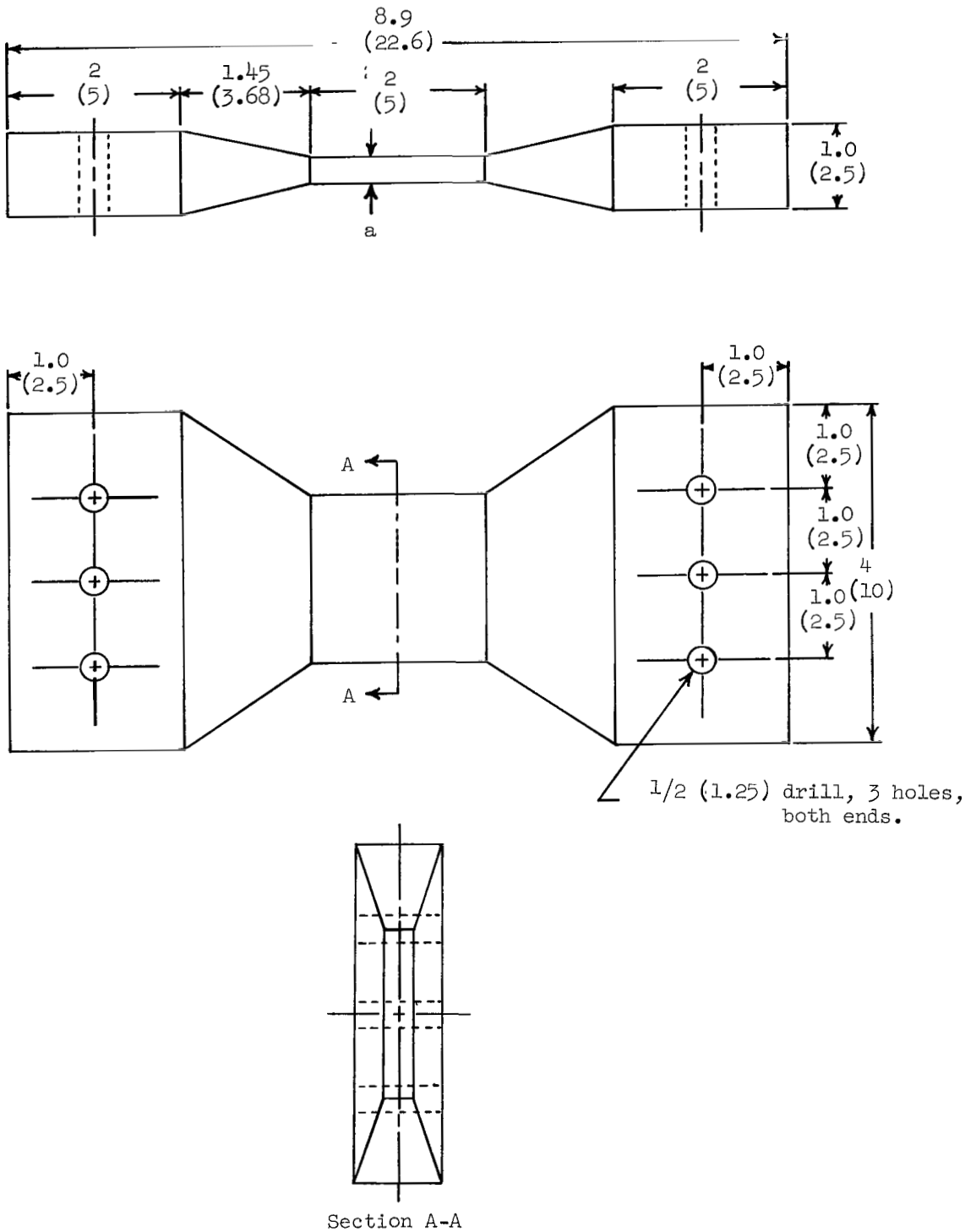

Figure 3.- Sketch of porous-carbon specimen. All dimensions are in inches (cm).

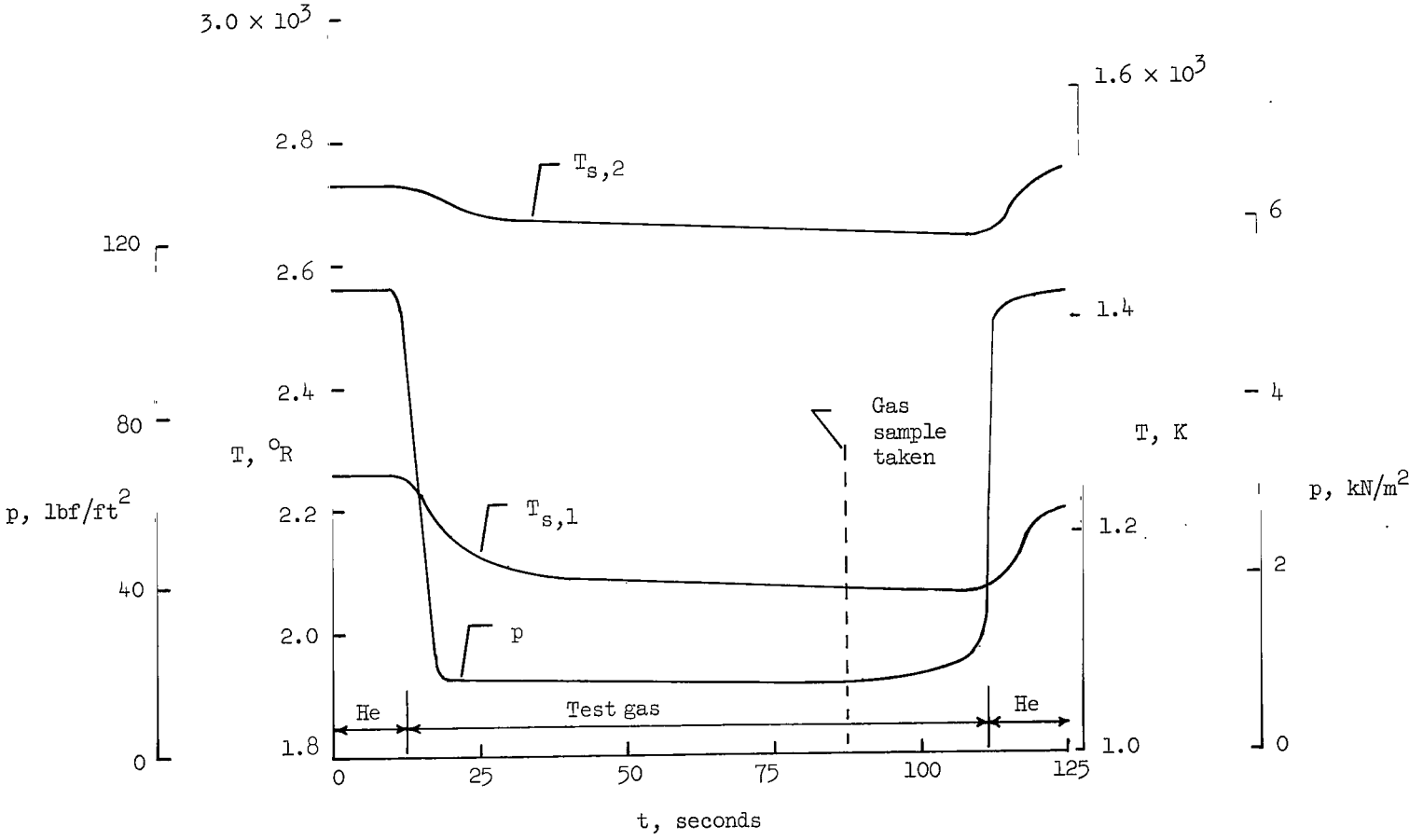

Figure 4.- Pressure and temperature history for a typical simulation of pyrolysis-gas flow through an ablator char. Grade 25 porous carbon; test 9; test gas, methane; $\dot{m}$ = 0.039 lbm/ft^2-sec (0.190 kg/m^2-sec); t = 0.025 ft (0.762 cm).

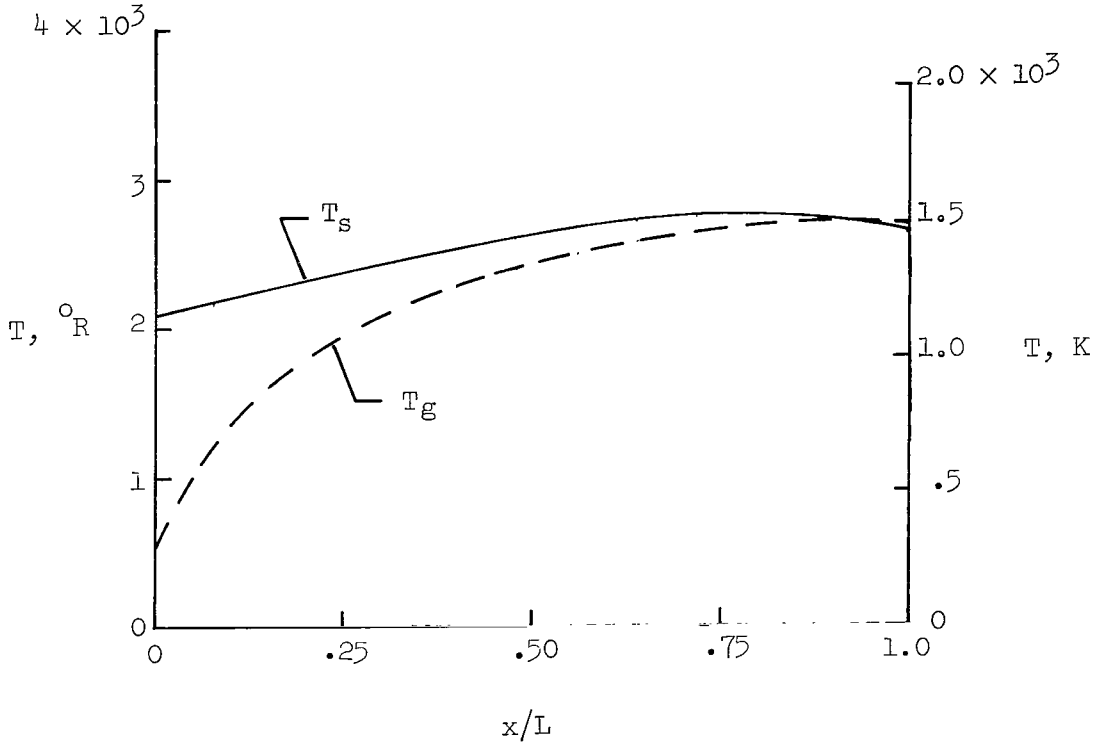

Figure 5.- Computed temperature profiles for a typical simulation of pyrolysis-gas flow through an ablator char. Grade 25 porous carbon; test 9; test gas, methane; $\dot{m}$ = 0.039 lbm/ft^2-sec (0.190 kg/m^2-sec); t = 0.025 ft (0.762 cm).

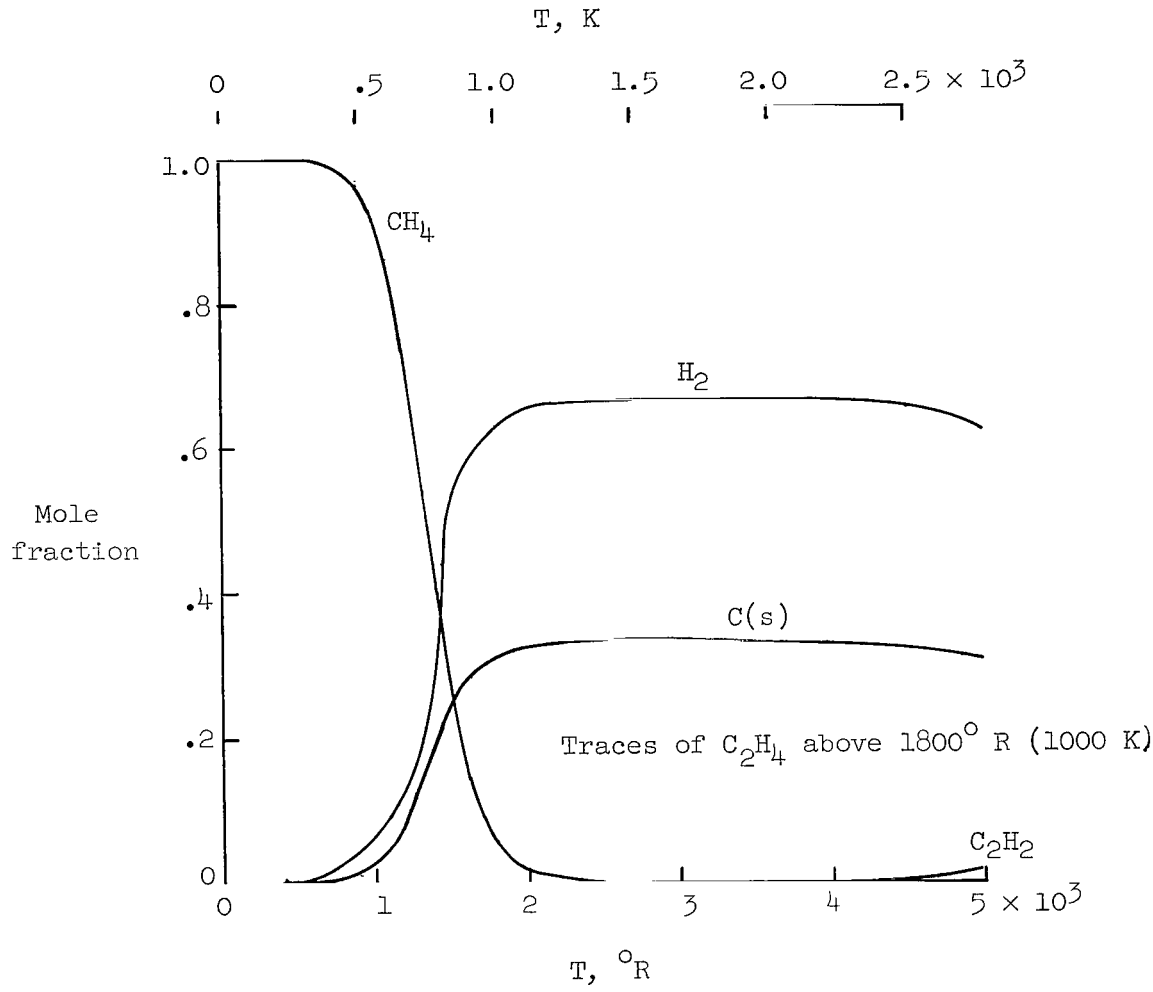

Figure 6.- Equilibrium chemical composition as a function of temperature for methane at a pressure of 1 atm.

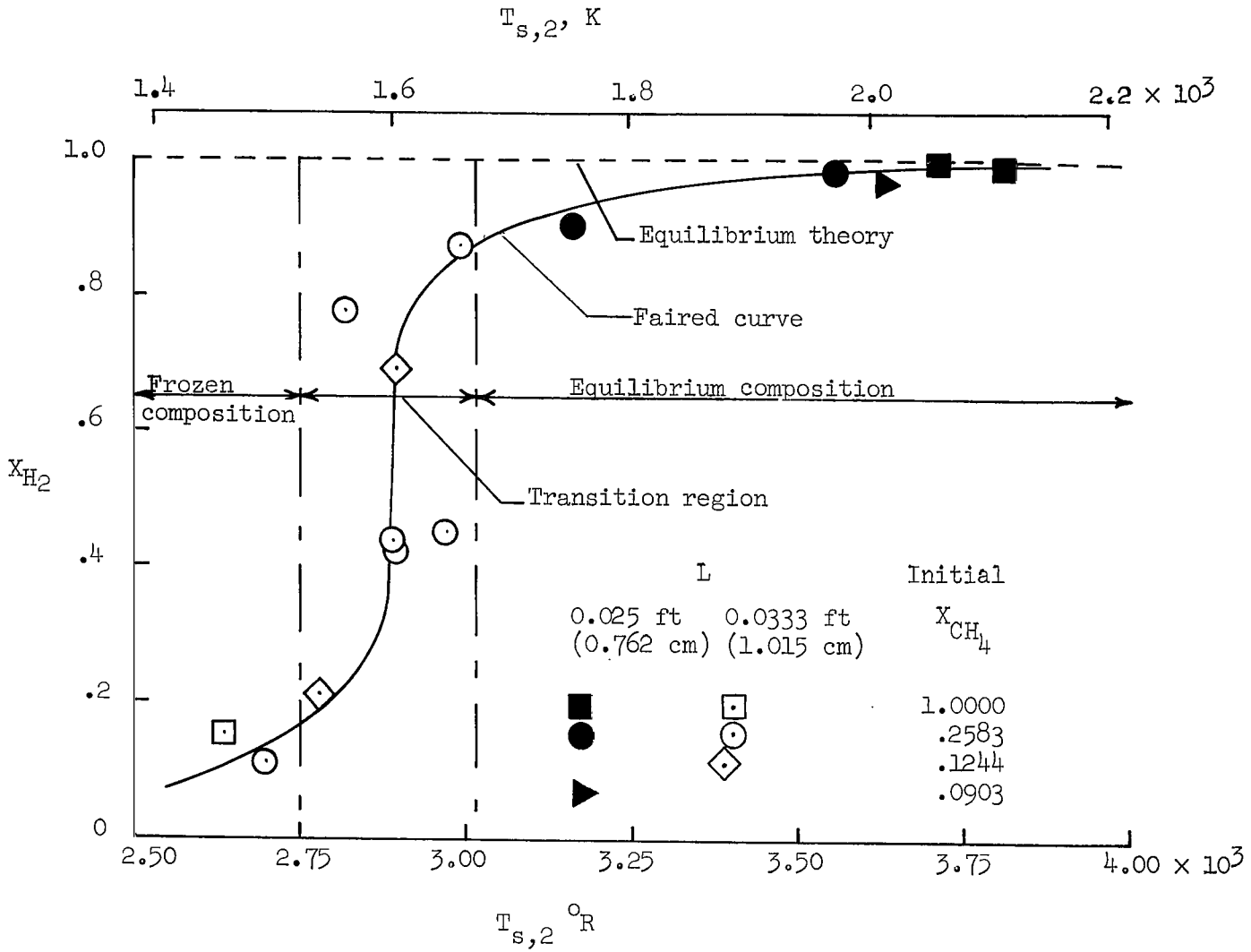

(a) Grade 25 porous carbon.

Figure 7.- Hydrogen mole fraction in test gas sample as a function of temperature at specimen exit surface for simulated flow through an ablator char.

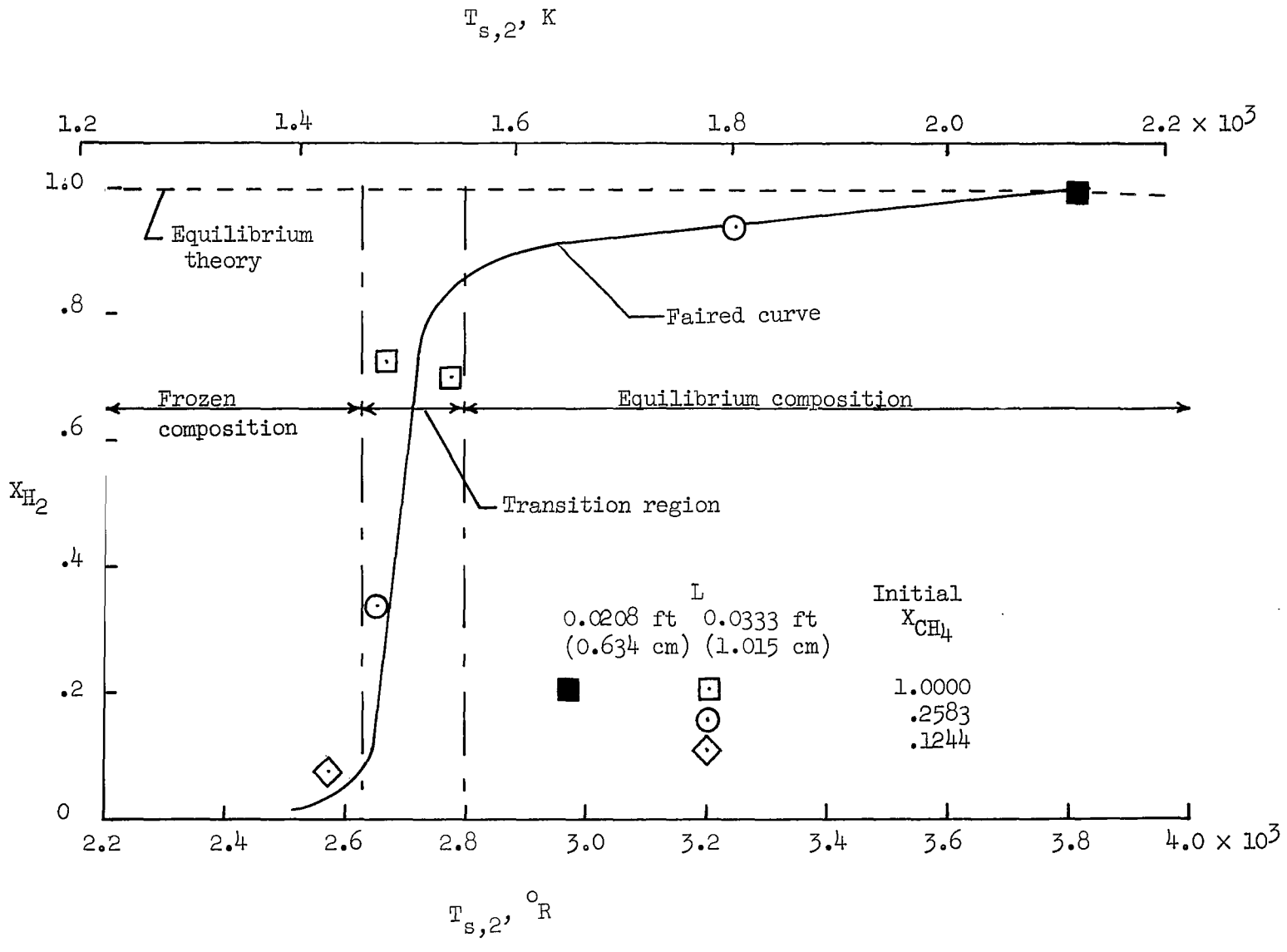

(b) Grade 45 porous carbon.

Figure 7.- Concluded.

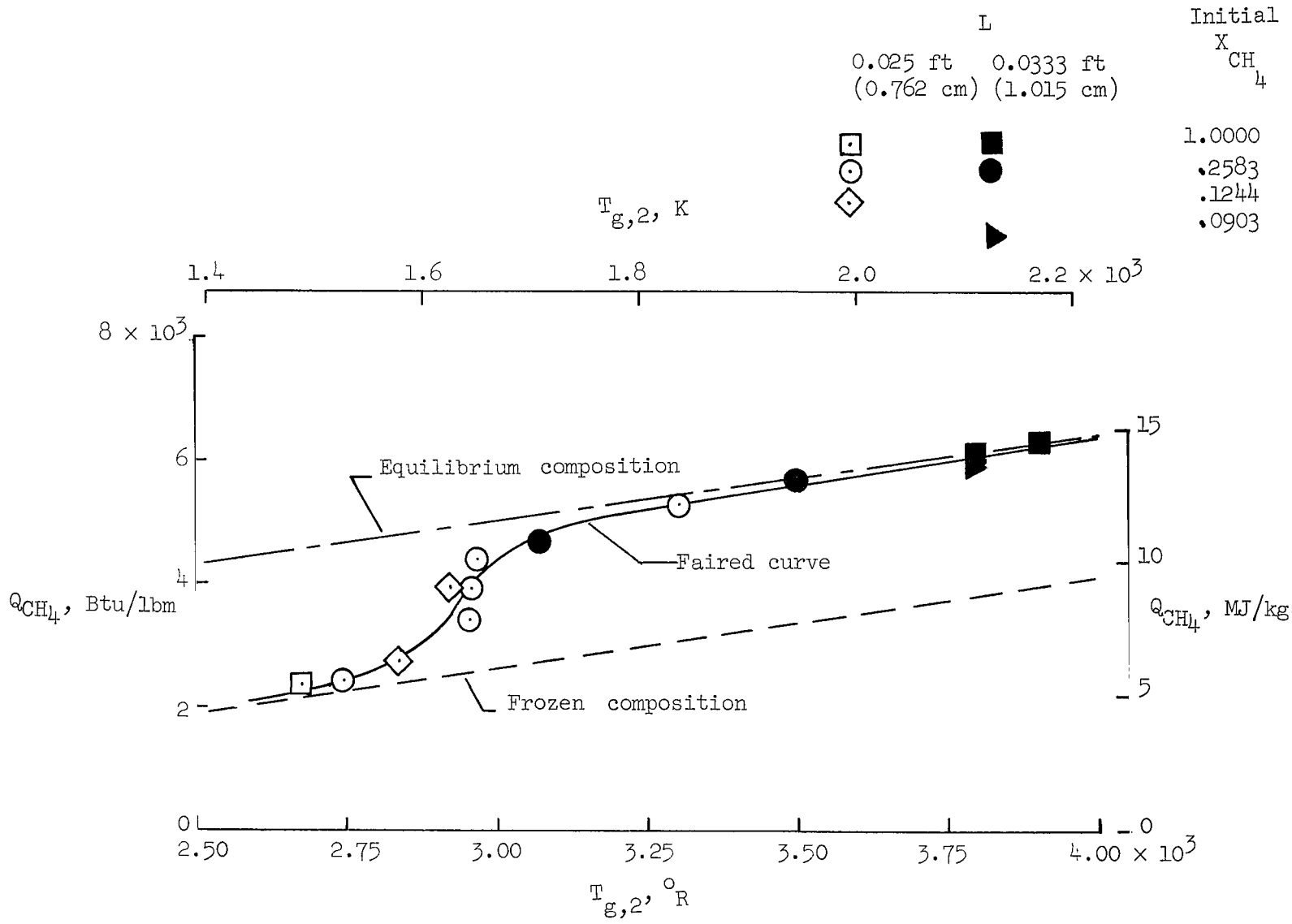

(a) Grade 25 porous carbon.

Figure 8.- Computed energy absorption by test gas as a function of gas temperature for simulated flow through an ablator char.

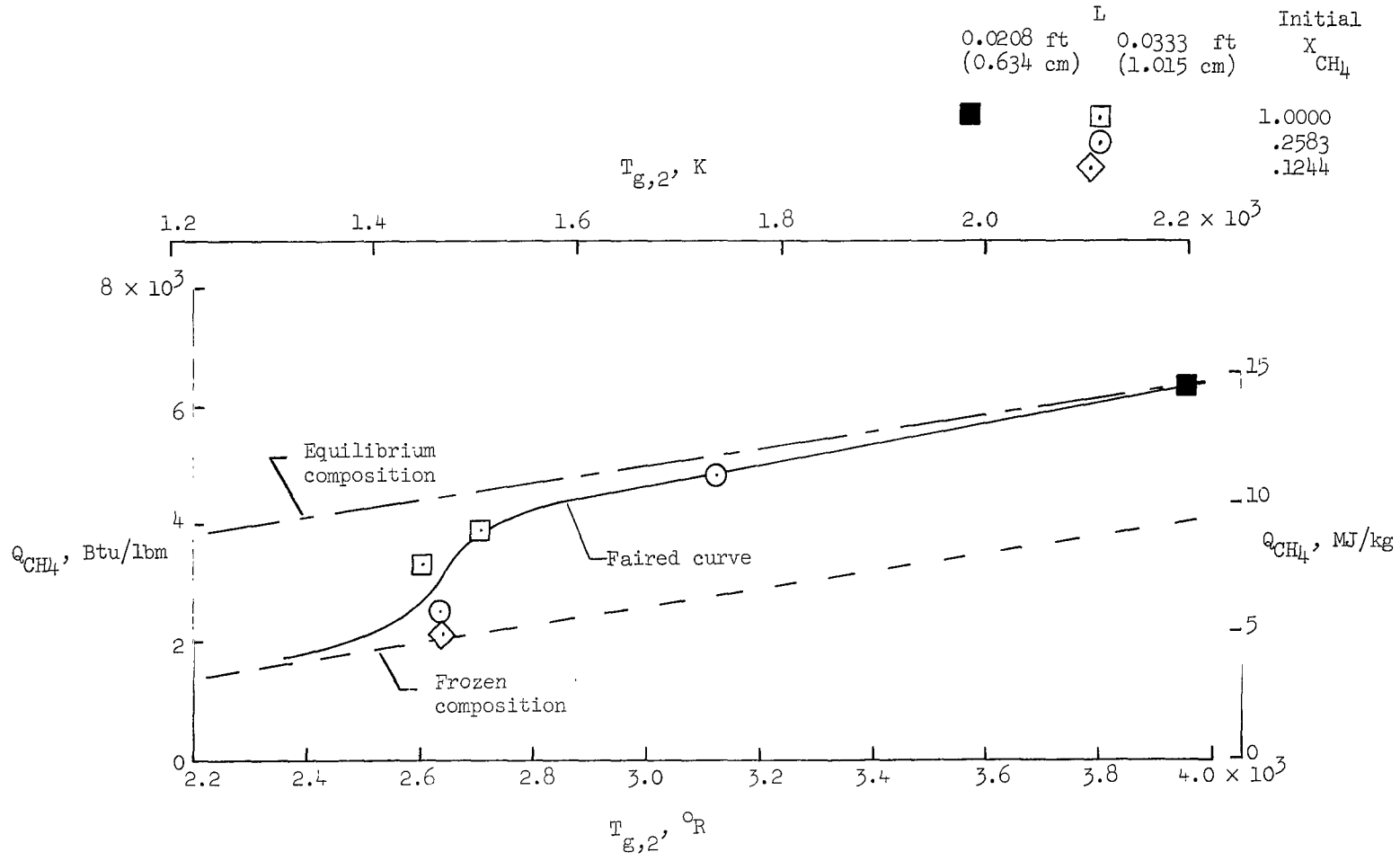

(b) Grade 45 porous carbon.

Figure 8.- Concluded.

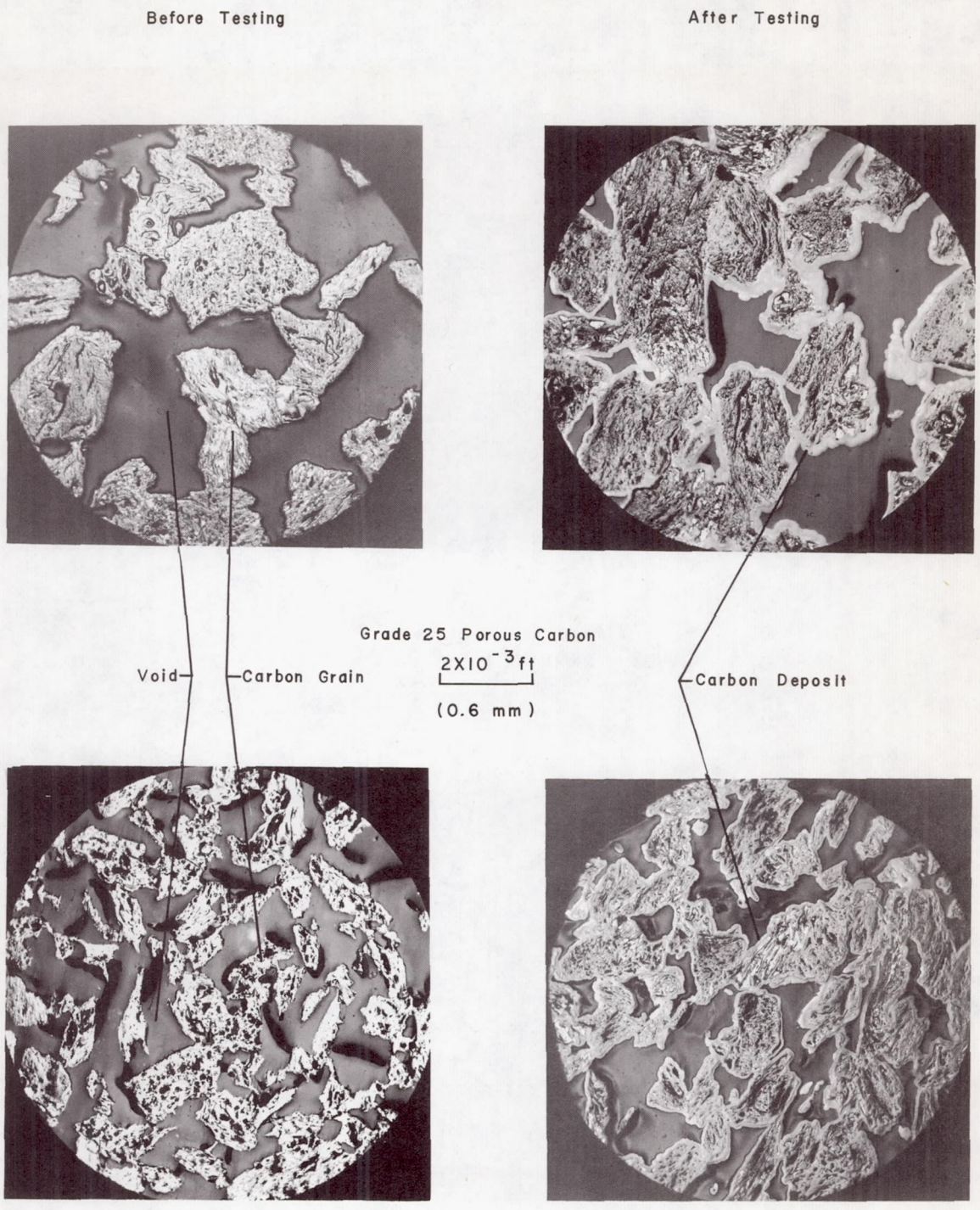

Figure 9.- Photomicrographs of simulated char before and after subjecting to test gas flow. L-69-5256

Figure 10.- Detailed photomicrograph of simulated char (grade 25 porous carbon) subjected to test gas flow. L-69-5257

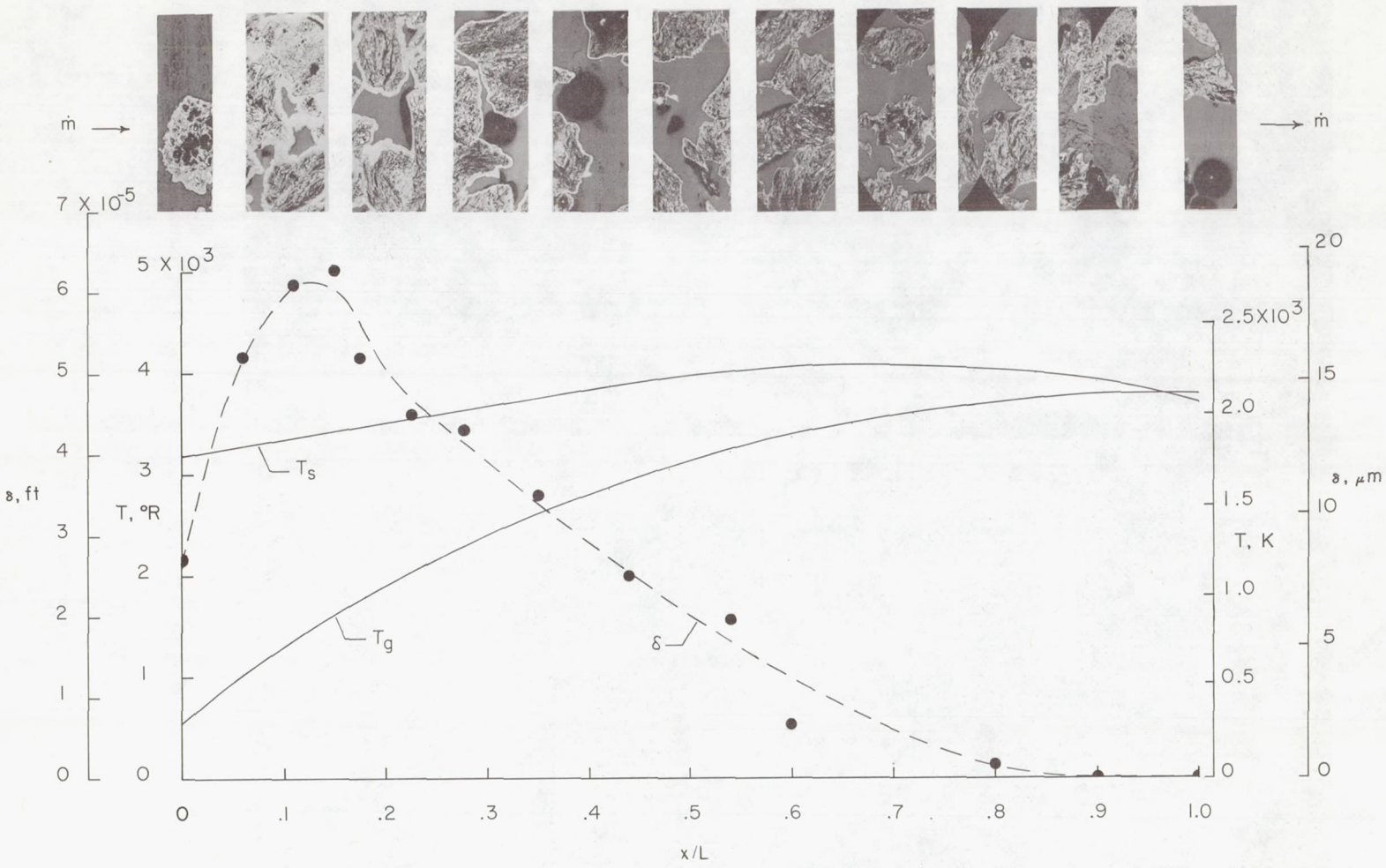

Figure 11.- Measured deposition and calculated temperature profile for a simulated char (grade 25 porous carbon, test 2) subjected to test gas flow. Specimen thickness, 0.33 ft (1.015 cm); test gas, methane; flow rate, 0.033 lbm/ft^2-sec (0.161 kg/m^2-s).

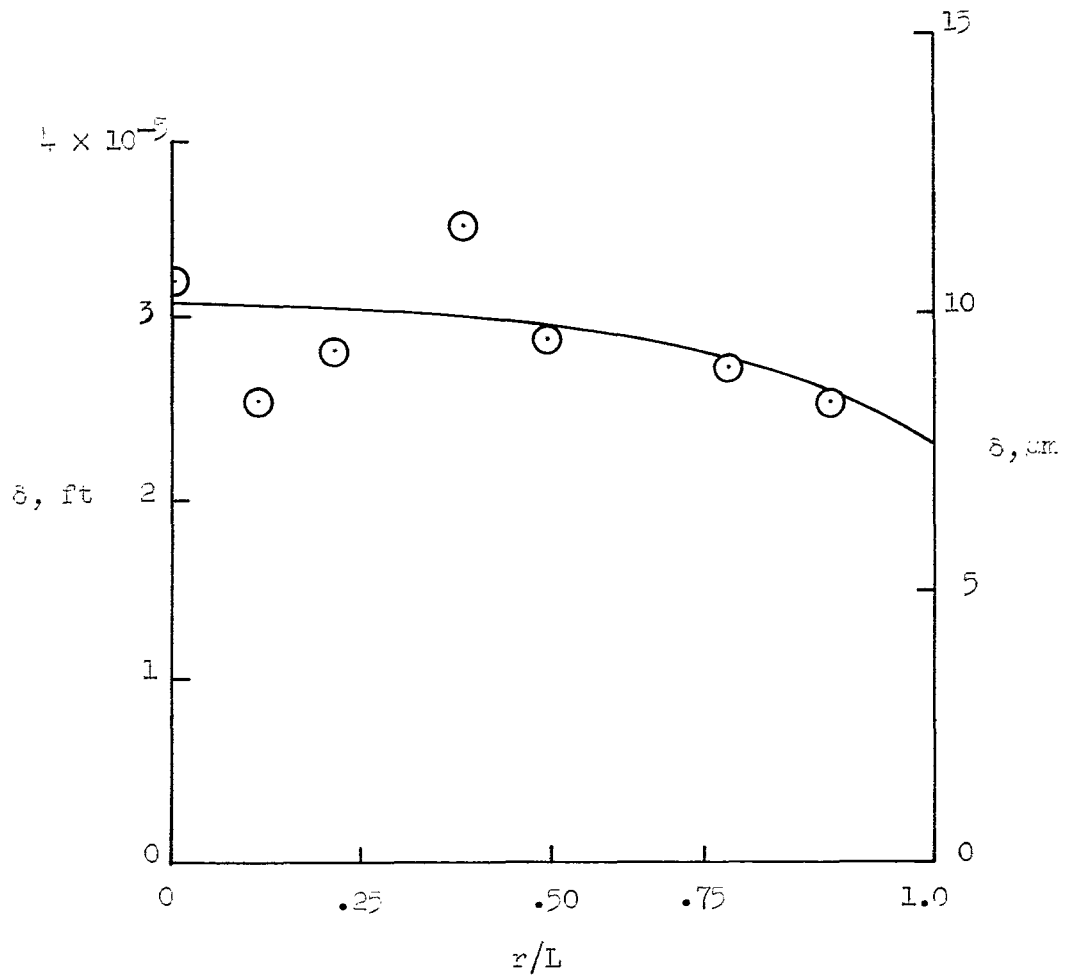

Figure 12.- Radial deposition profile for simulated char subjected to test gas flow. Grade 25 porous carbon; test 4.

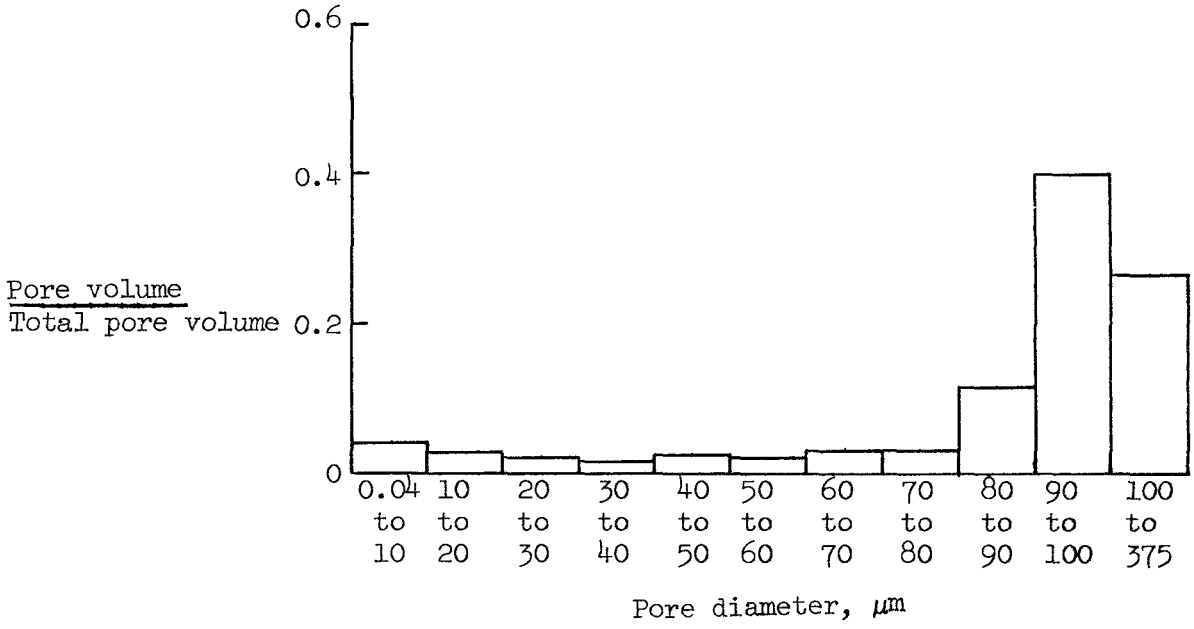

(a) Grade 25 porous carbon. d = 119 μm.

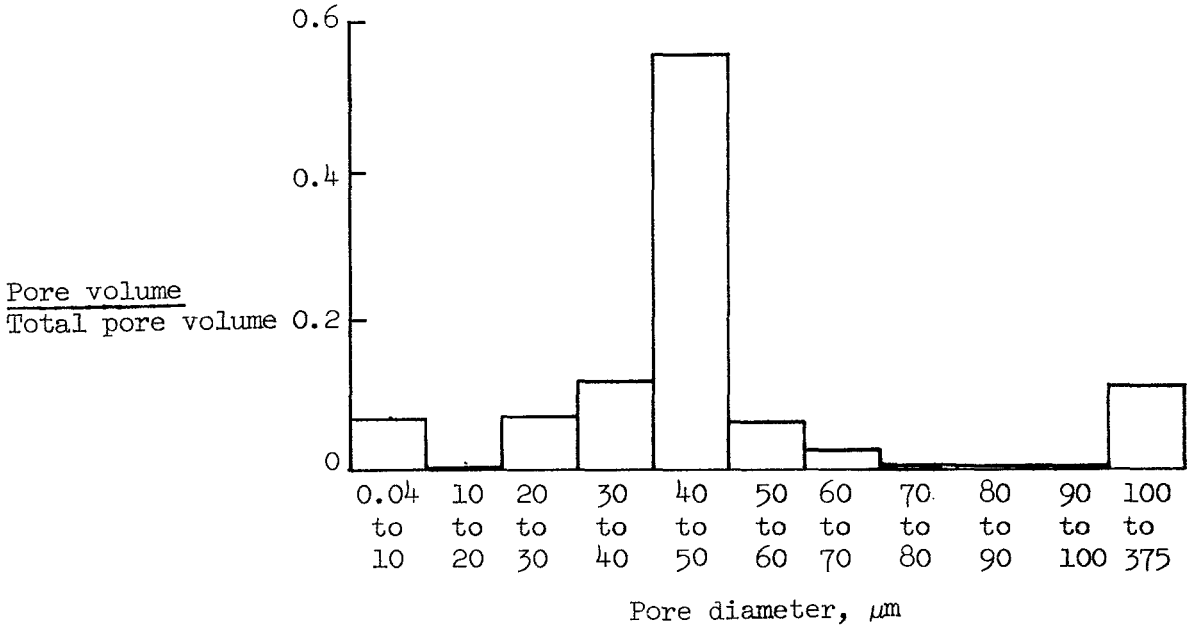

(b) Grade 45 porous carbon. d = 67 μm.

Figure 13.- Pore spectrum of simulated chars before subjecting to test gas flow. $\eta = 0.47$.

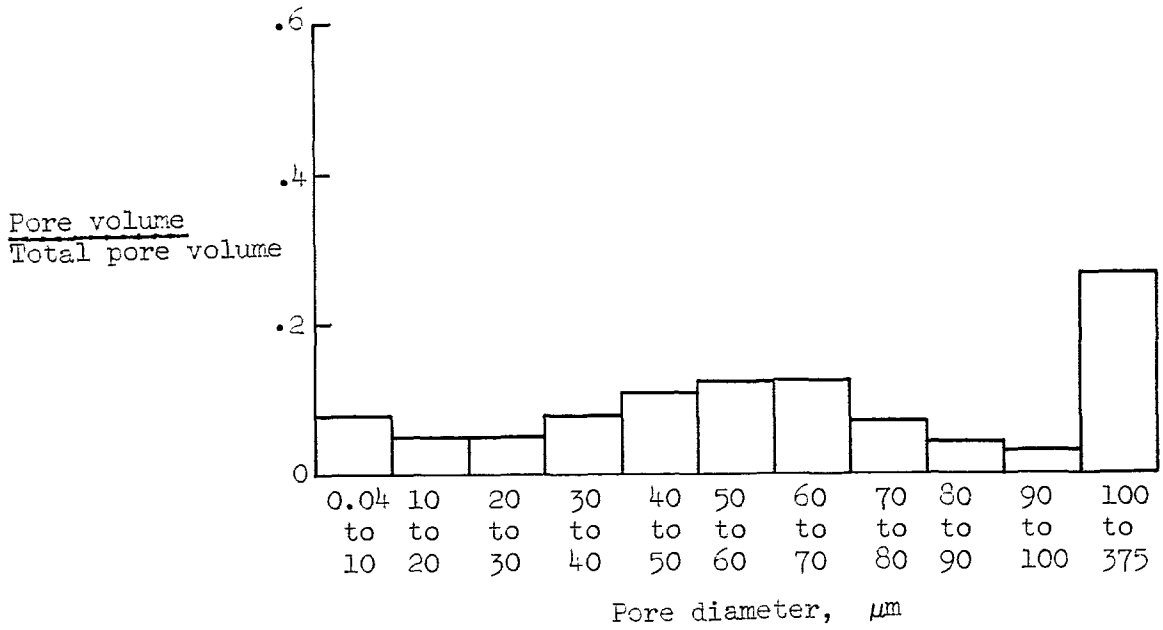

(a) Region $0 < x/L < 0.5$. $\eta = 0.32$; $d = 98$ μm.

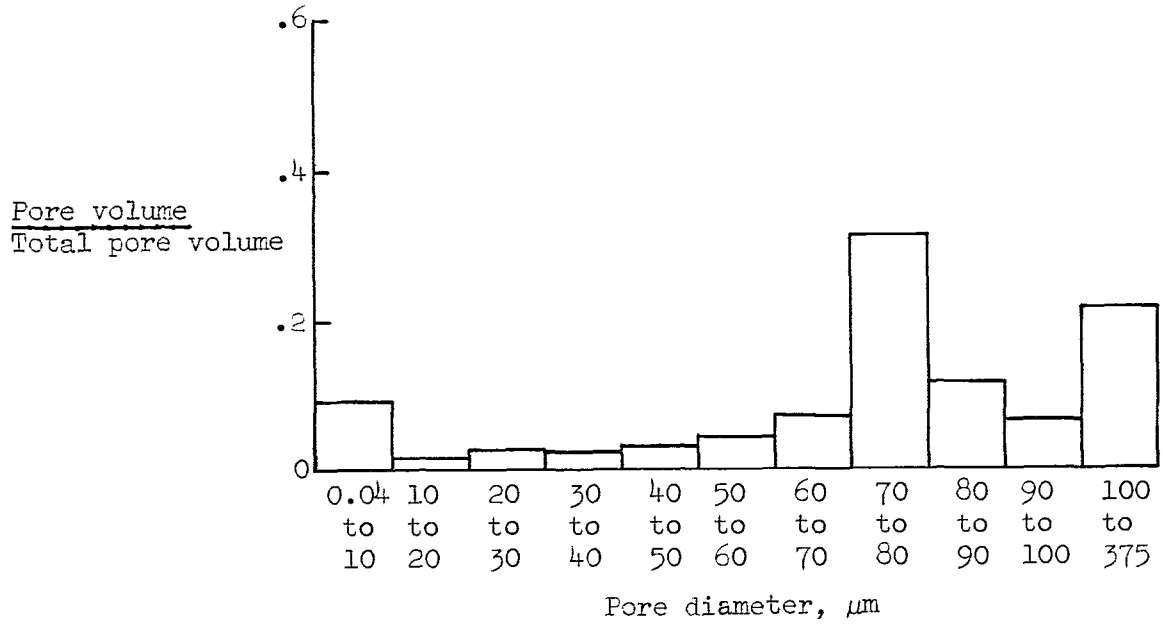

(b) Region $0.5 < x/L < 1.0$. $\eta = 0.45$; $d = 102$ μm.

Figure 14.- Pore spectrum of a simulated char (grade 25 porous carbon, test 2) after subjecting to test gas flow.

NATIONAL AERONAUTICS AND SPACE ADMINISTRATION
WASHINGTON, D. C. 20546
OFFICIAL BUSINESS

FIRST CLASS MAIL

POSTAGE AND FEES PAID
NATIONAL AERONAUTICS AND
SPACE ADMINISTRATION

POSTMASTER: If Undeliverable (Section 158 Postal Manual) Do Not Return

"The aeronautical and space activities of the United States shall be conducted so as to contribute . . . to the expansion of human knowledge of phenomena in the atmosphere and space. The Administration shall provide for the widest practicable and appropriate dissemination of information concerning its activities and the results thereof."

—NATIONAL AERONAUTICS AND SPACE ACT OF 1958

NASA SCIENTIFIC AND TECHNICAL PUBLICATIONS

TECHNICAL REPORTS: Scientific and technical information considered important, complete, and a lasting contribution to existing knowledge.

TECHNICAL NOTES: Information less broad in scope but nevertheless of importance as a contribution to existing knowledge.

TECHNICAL MEMORANDUMS: Information receiving limited distribution because of preliminary data, security classification, or other reasons.

CONTRACTOR REPORTS: Scientific and technical information generated under a NASA contract or grant and considered an important contribution to existing knowledge.

TECHNICAL TRANSLATIONS: Information published in a foreign language considered to merit NASA distribution in English.

SPECIAL PUBLICATIONS: Information derived from or of value to NASA activities. Publications include conference proceedings, monographs, data compilations, handbooks, sourcebooks, and special bibliographies.

TECHNOLOGY UTILIZATION PUBLICATIONS: Information on technology used by NASA that may be of particular interest in commercial and other non-aerospace applications. Publications include Tech Briefs, Technology Utilization Reports and Notes, and Technology Surveys.

Details on the availability of these publications may be obtained from:

SCIENTIFIC AND TECHNICAL INFORMATION DIVISION

NATIONAL AERONAUTICS AND SPACE ADMINISTRATION

Washington, D.C. 20546